**EURASIAN JOURNAL OF MATHEMATICAL AND COMPUTER APPLICATIONS**
ISSN 2306–6172
Volume 13, Issue 1 (2025) 154– 168

# A MULTISCALE MODEL REDUCTION PROCEDURE FOR NEUTRON TRANSPORT PROBLEMS

**Spiridonov D. A.**

**Abstract** For neuron transport modeling, the neutron transport $SP_3$ approximation is significantly more advantageous than using neutron diffusion. The $SP_3$ approximation is very efficient approach, because we can find some balance between accuracy and computational cost. The $SP_3$ model is fast and gives good level of accuracy. The $SP_3$ has a similar structure that a common approaches, like diffusion methods in $S_N$ or $P_N$ models. In this study we show a new strategy of solving a neutron transport problem for two group of neutrons. Our approach is based on generalized finite element method(GMsFEM). This approach involves constructing a special multiscale space on a coarse grid and projecting the original system onto a new space. This space is defined by special spectral basis functions. We construct an offline multiscale basis functions for each group of neutrons. The main problem has a multiscale nature and the multiscale bases can desctribe each heterogeneity of computational domain at micro-scale level. To show the applicability of the proposed approach, we compare the results with the exact solution obtained using the finite element method on a very fine mesh.

**Key words:** neutron transport equation, SP3 approximation, eigenvalue problem, multiscale simulation, generalized multiscale finite element method, GMsFEM.

**AMS Mathematics Subject Classification:** 65K05, 76M50.

**DOI:** 10.32523/2306-6172-2025-13-1-154-168

# 1 Introduction

One of the most important physical forms occurring inside a nuclear reactor is the movement of neutrons [1]. Complex integro-differential conditions are included to predict the propagation of neutrons. The condition of neutron flux depends on many features of physical process: for exmaple, heterogeneity of computational domain, inner energy of neutrons and the accuracy of computations [2]. Common sense calculations for nuclear reactors typically employ several types of approximations to neutron transit parameters. For example, most neutron codes rely on multigroup diffusion equations. A computational illustration may be the creation of a connected second-order parabolic equation, followed by the creation of standard differential conditions that need the addition of delayed neutrons.

A nuclear reactor usually has a critical equilibrium state in which the balance of absorption and production of neutrons is maintained; such a state is called steady state. Such a special state is described using a lambda spectral problem, assuming that the desired eigenvalue is maximum, that called the k-effective nucleus, is equal

to one [3, 4, 5]. In this case, the steady neutron field is assigned a corresponding eigenfunction. The calculation of a reactor with efficiency using the lambda mode problem is important for the design of the reactor.

To calculate a real application problem when modeling a nuclear reactor, it is usually necessary to construct very detailed fine grids, especially if the process lasts for a long time, then we are faced with the problem of a very large number of time layers. And since the processes in the reactor occur very quickly, we have to take a very small time step in order not to miss any critical jumps in the state. Therefore, such complex application problems require very powerful computers, which are not available to everyone. Numerical averaging methods or various multiscale methods are usually used to solve such problems. This technique allows us to significantly reduce the size of the original problem and makes it possible to solve the problem even on low-performance systems that everyone has. Also, for the non-stationary problem of neuron diffusion, various methods for space and time factorization are often used, also with the aim of reducing the computational cost [6, 7]. In the following work [8] the authors develop a general strategy for obtaining approximate solutions to non-stationary neutron transfer problems with an emphasis on fast calculations using state-change methods.

Homogenization methods allow to save computational resources by solving the problem on a very coarse grid. These methods imply solving local problems in order to find special macroscopic properties of the medium by solving local problems at the micro level. As a result, we obtain a set of macroscopic parameters, based on which we can build an approximation on a coarse grid [9, 10, 11, 12]. In this approach, only a one-way connection between the micro- and macro- scales is defined. Multiscale methods provide a mutual connection between the micro- and macro- scales. This approach is possible due to special basis functions that are linked in a global coarse-grid formulation to form a new multiscale space on which the entire approximation is built. There are many variations of this method, and everything depends on the type of multiscale basis functions. Some of the types of multiscale functions are presented in the following paper [13].

The current study utilizes multiscale modeling techniques to minimize the computational demands associated with the high dimensionality of the initial problem [14, 15, 16]. One of the most recognized and widely employed techniques is the multiscale finite element method (MsFEM) [13, 17, 16]. In problems with complex geometry of the domain, where very high jumps of values occur, the usual MsFEM has very poor accuracy. For this, it is necessary to describe the microscale properties of the medium at the macro level in more detail, for this, the Generalized Multiscale Finite Element Method is well suited, which can use several multiscale bases to describe one local region. By solving the spectral problem, one local basis can be constructed for each microscale characteristic [18, 19, 20, 21, 22]. By adapting the finite volume method, researchers developed the multiscale finite volume method (MsFVM) [23, 24, 25]. An effective approach for solving fluid flow challenges in porous media is the mixed multiscale finite element method (Mixed-MsFEM) [26, 27].

For problems with complex heterogeneity such as cracks and channels, it is recommended to use multiscale methods with domain oversampling. One of such methods

is the Constrainted Energy Minimizing Generalized Finite Multiscale Element Method (CEM-GMsFEM) which builds special basic functions that contain information about the process in neighboring local areas, local areas in this method are built with expansion [28, 29, 30, 31]. Also, in applications, multicontinuum problems with a high value of flows between continua are often encountered; for such problems, coupled multiscale basis functions are suitable. These bases store information about all continua and provide a more accurate approximation [32, 22, 33].

We present a new algorithm of the multiscale method, which is built on the basis of the generalized multiscale finite element method [34, 35]. We will apply this algorithm to solve the problem of neuron transport in a heterogeneous medium (the active zone of a nuclear reactor). This algorithm includes only two stages. We start building the algorithm from the offline stage. This stage is preparatory, here we define the multiscale space. The multiscale space is a linear shell of the basis functions that are built in each local subdomain. To identify multiscale basis functions, we first develop local spectral problems, which allow us to express local micro-characteristics by employing a collection of bases. The second stage is the online stage, at which we solve a low-dimensional system on a predetermined multiscale space.

The paper organized as follows, in Section 2, we show a problem formulation and approximation on the fine grid by finite element method for 2D small PWR test with two group of neutrons. In Section 3, we present and algorith of GMsFEM, where we demonstrate an offline bases construction for each group on neutrons. Finally, in Section 4, we depict a numerical results for test with one group of neutrons and for test with two group of neutrons. We compare solution and integral power that obtained with GMsFEM with reference fine grid solution.

## 2 Problem statement

We discuss neutron transport, which is characterized by symmetric neutron flux equations in the $SP_3$ form. We analyze the problem in a two-dimensional or three-dimensional symmetric domain $\Omega$ ($\boldsymbol{x} = \{x_1, ..., x_d\} \in \Omega$, $d = 2, 3$) with a boundary $\partial\Omega$. The neutron transport model is presented below:

$$\begin{aligned}
\frac{1}{v_g}\frac{\partial\phi_{0,g}}{\partial t} - \frac{2}{v_g}\frac{\partial\phi_{2,g}}{\partial t} - \nabla\cdot D_{0,g}\nabla\phi_{0,g} + \Sigma_{r,g}\phi_{0,g} - 2\Sigma_{r,g}\phi_{2,g} \\
= (1-\beta)\chi_{n,g}S_n + S_{s,g} + \chi_{d,g}S_d, \\
-\frac{2}{v_g}\frac{\partial\phi_{0,g}}{\partial t} + \frac{9}{v_g}\frac{\partial\phi_{2,g}}{\partial t} - \nabla\cdot D_{2,g}\nabla\phi_{2,g} + 5\Sigma_{t,g} + 4\Sigma_{r,g})\phi_{2,g} - 2\Sigma_{r,g}\phi_{0,g} \\
= -2(1-\beta)\chi_{n,g}S_n - 2S_{s,g} - 2\chi_{d,g}S_d,
\end{aligned} \tag{1}$$

where

$$S_n = \sum_{g'=1}^{G}\nu\Sigma_{f,g'}\phi_{g'}, \quad S_{s,g} = \sum_{g\neq g'=1}^{G}\Sigma_{s,g'\to g}\phi_{g'}, \quad S_d = \sum_{m=1}^{M}\lambda_m c_m,$$

$$\phi_{0,g} = \phi_g + 2\phi_{2,g}, \quad D_{0,g} = 1/3\Sigma_{tr,g}, \quad D_{2,g} = 9/7\Sigma_{t,g}, \quad g = 1, 2, \ldots, G.$$

Here $G$ – number of energy groups, $M$ – number of types of delayed neutrons, $\Sigma_{t,g}(\boldsymbol{x}, t)$ – total cross-section, $\Sigma_{tr,g}(\boldsymbol{x}, t)$ – transport cross-section, $\phi_{0,g}(\boldsymbol{x}, t)$ – pseudo 0th moment of angular flux, $\phi_g(\boldsymbol{x}, t)$ – scalar flux, $\phi_{2,g}(\boldsymbol{x}, t)$ – second moment of angular flux,

$\Sigma_{r,g}(\boldsymbol{x},t)$ – removal cross-section, $\Sigma_{s,g'\to g}(\boldsymbol{x},t)$ – scattering cross-section, $\nu\Sigma_{f,g}(\boldsymbol{x},t)$ – generation cross-section, $\chi_g$ – spectra of neutrons, $\lambda_m$ – decay constant of delayed neutron sources. $c_m(\boldsymbol{x},t)$ – density of sources of delayed neutrons.

The equations that presented below, define the density of sources of delayed neutrons.

$$\frac{\partial c_m}{\partial t} + \lambda_m c_m = \beta_m S_n, \quad m = 1, 2, \ldots, M, \tag{2}$$

where $\beta = \sum_{m=1}^{M} \beta_m$ is the fraction of delayed neutrons of m-type.At the boundary $\partial\Omega$ of the computational domain we define vacuum Marshak-type boundary conditions

$$\begin{bmatrix} J_{0,g}(\boldsymbol{x}) \\ J_{2,g}(\boldsymbol{x}) \end{bmatrix} = \begin{bmatrix} 1/2 & -3/8 \\ -3/8 & 21/8 \end{bmatrix} \begin{bmatrix} \phi_{0,g}(\boldsymbol{x}) \\ \phi_{2,g}(\boldsymbol{x}) \end{bmatrix}, \qquad J_{i,g}(\boldsymbol{x}) = -D_{i,g}\nabla\phi_{i,g}(\boldsymbol{x}), \quad i = 0, 2. \tag{3}$$

As an initial condition, we take the equilibrium state of the reactor

$$\phi_g(\boldsymbol{x}, 0) = \phi_g^0(\boldsymbol{x}), \quad g = 1, 2, \ldots, G, \qquad c_m(\boldsymbol{x}, 0) = c_m^0(\boldsymbol{x}), \quad m = 1, 2, \ldots, M. \tag{4}$$

**Discretization.** Let's discretize the boundary problem (1)-(4). We generate a uniform unstructured grid

$$\omega = \{t^n = n\tau, \quad n = 0, 1, \ldots, N, \quad \tau N = T\}$$

and make use of the following notations Let $c_m^n = c_m(\boldsymbol{x}, t^n)$ and $\phi_g^n = \phi_g(\boldsymbol{x}, t^n)$. Using a finite-difference technique, we discretize the time derivatives of equation (1). For the time approximation, we employ a fully implicit method with a time step of $\tau$. We establish time approximations for the delayed neutron source equation using a numerical-analytical approach. The equivalent form of the equation (2)

$$\frac{\partial e^{\lambda_m t} c_m}{\partial t} = \beta_m e^{\lambda_m t} \sum_{g=1}^{G} \nu\Sigma_{fg}\phi_g, \quad m = 1, 2, \ldots, M.$$

In the time interval $[t^n, t^{n+1}]$ we have the following integration

$$c_m^{n+1} = e^{-\lambda_m \tau} c_m^n + \beta_m \int_{t_n}^{t_{n+1}} e^{\lambda_m (t - t^{n+1})} \sum_{g=1}^{G} \nu\Sigma_{fg}\phi_g dt, \quad m = 1, 2, \ldots, M. \tag{5}$$

We take the integrand on the right side of (5) at $t = t^{n+1}$ when employing the fully implicit technique.

For the spatial approximation, we employ the finite element approach. In the Sobolev space $H^1(\Omega)$, $q \in H^1$: $q^2$ and $|\nabla q|^2$ have a finite integral in $\Omega$. The following variational formulation is obtained by applying the integration by parts: In $V^G$, let's identify $\phi_g^{n+1}$ such that

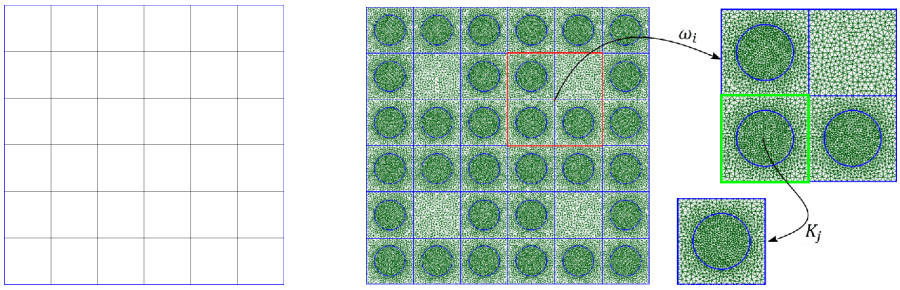


Figure 1: Coarse grid and local domain $\omega_i$ with $K_j$

$$\begin{aligned}
&\int_\Omega \left( \frac{\phi_{0,g}^{n+1} - \phi_{0,g}^{n}}{v_g \tau} - \frac{2(\phi_{2,g}^{n+1} - \phi_{2,g}^{n})}{v_g \tau} \right) q_g d\boldsymbol{x} - \int_\Omega D_{0,g} \nabla \phi_{0,g}^{n+1} \nabla q_g d\boldsymbol{x} \\
&\qquad + \int_{\partial\Omega} J_{0,g}^{n+1} q_g d\boldsymbol{s} + \int_\Omega (\Sigma_{r,g} \phi_{0,g}^{n+1} - 2\Sigma_{r,g} \phi_{2,g}^{n+1}) q_g d\boldsymbol{x} \\
&\qquad = \int_\Omega ((1-\beta)\chi_{n,g} S_n^{n+1} + S_{s,g}^{n+1} + \chi_{d,g} S_d^{n+1}) q_g d\boldsymbol{x}, \\
&\int_\Omega \left( -\frac{2(\phi_{0,g}^{n+1} - \phi_{0,g}^{n})}{v_g \tau} + \frac{9(\phi_{2,g}^{n+1} - \phi_{2,g}^{n})}{v_g \tau} \right) q_g d\boldsymbol{x} - \int_\Omega D_{2,g} \nabla \phi_{2,g}^{n+1} \nabla q_g d\boldsymbol{x} \\
&\qquad + \int_{\partial\Omega} J_{2,g}^{n+1} q_g d\boldsymbol{s} + \int_\Omega ((5\Sigma_{t,g} + 4\Sigma_{r,g}) \phi_{2,g}^{n+1} - 2\Sigma_{r,g} \phi_{0,g}^{n+1}) q_g d\boldsymbol{x} \\
&\qquad = \int_\Omega (-2(1-\beta)\chi_{n,g} S_n^{n+1} - 2S_{s,g}^{n+1} - 2\chi_{d,g} S_d^{n+1}) q_g d\boldsymbol{x},
\end{aligned} \tag{6}$$

where $V^G = [H^1(\Omega)]^G$.

Additionally, a transition from the continuous variational problem (6) to the discrete problem is required. We formulate a discrete variational issue and introduce a finite-dimensional space with finite elements $V_h^G \subset V^G$. The problem on the fine grid is solved using ordinary linear basis functions as basis functions. We get a set of linear algebraic equations, presented below.

$$A_f \phi = b_f, \tag{7}$$

where the vector $b_f$ represents the linear form of equation (6), and the operator $A_f$ represents the bilinear form of the equation. Note that we employ the scheme of two groups of neutrons $G = 2$ in our implementation.

# 3 Model reduction algorithm

We employ GMsFEM for coarse grid discretization. We create two grids (see Fig. 1): fine ($\mathcal{T}_h$) and coarse ($\mathcal{T}_H$). To generate multiscale basis, we build local domains $\omega_i$, where $i = 1, ..., N_v$ and $N_v$ indicates the number of coarse grid nodes. Given a refinement of $\mathcal{T}_H$, $h$ and $H$ denote fine and coarse grid sizes, respectively. The coarse grid $\mathcal{T}_H$ contains numerous fine-scale characteristics, but we presume that the fine-scale grid $\mathcal{T}_h$ is fine enough to properly resolve the domain's small-scale information. The coarse cells around one vertex of the coarse grid are linked to form a local domain $\omega_i$.

The multiscale function spaces are constructed in the following form

$$V_{\text{off}} = \text{span}\{y_g^i\}, \quad i = 1..N_c, \quad g = 1, 2.$$

The number of coarse basis functions is represented by $N_c$. Each local domain $w_i$ contains a collection of bases $y_g^i$.

The purpose of basis functions is to represent the solution's multiscale characteristics. Localized basis functions, which include information about scales smaller (and larger) than the local numerical scale specified by the basis functions, capture important multiscale characteristics of the solution.

**Multiscale space.** Local spectral problems are used to compute basis functions by reducing the dimension of the local problem. We introduce a basic building for the two-neutron situation. Two kinds of multiscale basis functions must be constructed: one for the pseudo 0th moment and one for the second. The following spectral problem must be resolved in each local domain $\omega_i$ in order to obtain the set of multiscale basis functions

$$A_1\varphi_1^i = \lambda S_1\varphi_1^i, \qquad A_2\varphi_2^i = \lambda S_2\varphi_2^i, \tag{8}$$

where $A_1 = \{a_{ij}^1\}$ and $A_2 = \{a_{ij}^2\}$ are the matrices elements, and $S_1 = \{s_{ij}^1\}$, and $S_2 = \{s_{ij}^2\}$ are described as follows:

$$\begin{aligned}
a_{ij}^1 &= \int_{\omega_i} D_{0,1}\nabla\varphi_{0,1}\nabla q_1 d\boldsymbol{x} + \int_{\omega_i} (\Sigma_{r,1}\varphi_{0,1} - 2\Sigma_{r,1}\varphi_{2,1})q_1 d\boldsymbol{x} + \\
&+ \int_{\omega_i} D_{2,1}\nabla\varphi_{2,1}\nabla q_1 d\boldsymbol{x} + \int_{\omega_i} ((5\Sigma_{t,1} + 4\Sigma_{r,1})\varphi_{2,1} - 2\Sigma_{r,1}\varphi_{0,1})q_1 d\boldsymbol{x} \\
s_{ij}^1 &= \int_{\omega_i} D_{0,1}\nabla\varphi_{0,1}\nabla q_1 d\boldsymbol{x} + \int_{\omega_i} D_{2,1}\nabla\varphi_{2,1}\nabla q_1 d\boldsymbol{x} \\
a_{ij}^2 &= \int_{\omega_i} D_{0,2}\nabla\varphi_{0,2}\nabla q_2 d\boldsymbol{x} + \int_{\omega_i} (\Sigma_{r,2}\varphi_{0,2} - 2\Sigma_{r,2}\varphi_{2,2})q_2 d\boldsymbol{x} + \\
&+ \int_{\omega_i} D_{2,2}\nabla\varphi_{2,2}\nabla q_2 d\boldsymbol{x} + \int_{\omega_i} ((5\Sigma_{t,2} + 4\Sigma_{r,2})\varphi_{2,2} - 2\Sigma_{r,2}\varphi_{0,2})q_2 d\boldsymbol{x} \\
s_{ij}^2 &= \int_{\omega_i} D_{0,2}\nabla\varphi_{0,2}\nabla q_2 d\boldsymbol{x} + \int_{\omega_i} D_{2,2}\nabla\varphi_{2,2}\nabla q_2 d\boldsymbol{x}
\end{aligned} \tag{9}$$

Next, we generate the multiscale basis functions using the eigenvectors that correspond to the dominating $M_i$ eigenvalues from (8). We can see that we are computing multiscale basis functions for every group of neutrons separately from the equations (8)-(9). However, the multiscale bases are connected at the pseudo 0th and second moments for each distinct set of neutrons.

To generate conforming basis functions, we multiply eigenvectors associated with dominating eigenvalues by the partition of unity functions. In each domain $\omega_i$, we employ linear functions to partition unity functions $\chi_i$. In the domain $K_j$, partitions of unity are computed as a linear function from $\Gamma$ to vertex $A$. The segment $\Gamma$ is assigned the value 0, while point $A$ is allocated the value 1. This results in a linear function from 0 to 1 that spans the entire domain $K_j$. Figure 2 displays partitions of unity. Domain $K_j$ represents a single element from a coarse grid.

The linear shell of $y_1^i = \varphi_1^i\chi_i,\ y_2^i = \varphi_2^i\chi_i$, where $\chi_i$ is the typical nodal basis function for the node $i$ (linear partition of unity functions), is recognized as the multiscale space. Additionally, each multiscale basis function has two components: $y_1^i = (y_{0,1}^i, y_{2,1}^i),\ y_2^i =$

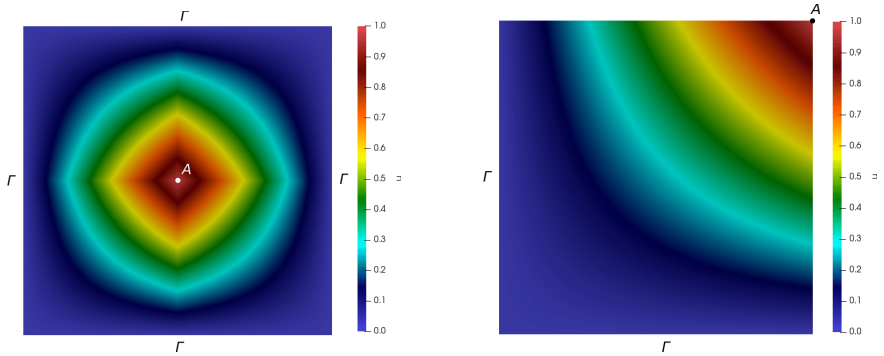

Figure 2: Partition of unity functions on the $\omega_i$ (right) and $K_j$ (left)

$(y^i_{0,2}, y^i_{2,2})$ for the pseudo 0th moment and $y^i_1 = (y^i_{0,1}, y^i_{2,1})$ for the second moment. The number of bases can vary, and increasing the number of bases can improve the solution's accuracy.

**Coarse-scale approximation.** The following matrix is then produced for every domain $\omega_i$

$$R^i_g = [y^1_g, \ldots, y^{M_i-1}_g, y^{M_i}_g], \ g = 1, 2, \ i = 1...N_v,$$

thus in order to lower the problem's dimension, we define the transition matrix $R$ between the fine and coarse grids

$$R = \begin{pmatrix} R_1 & 0 \\ 0 & R_2 \end{pmatrix}, \ R_1 = [R^1_1, R^2_1, \ldots, R^{N_v}_1], \ R_2 = [R^1_2, R^2_2, \ldots, R^{N_v}_2],$$

where the first and second groups of neutrons' multiscale basis functions are included in matrices $R_1$ and $R_2$, respectively, and $N_v$ is the number of local domains $\omega_i$.

Next, we build the coarse grid approximation using the fine grid system (7) and the transition matrix $R$, $A_c\phi_c = b_c$, $A_c = RA_fR^T$ and $b_c = Rb_f$, and using the coarse-scale solution $\phi_c = (\phi_{c_{0,1}}, \phi_{c_{2,1}}, \phi_{c_{0,2}}, \phi_{c_{2,2}})$, we can reconstruct the fine grid solution $\phi_{ms} = R^T\phi_c$, where $\phi_{ms} = (\phi_{ms_{0,1}}, \phi_{ms_{2,1}}, \phi_{ms_{0,2}}, \phi_{ms_{2,2}})$.

# 4 Numerical results

Non-stationary tests are numerically modeled in the transport $SP_3$ approximation. The generalized multiscale finite element method and the finite element method's numerical results are examined and contrasted. The FEniCS scientific library was used to develop the software. Asymmetric matrix spectrum problems have been resolved using the SLEPc package.

We compute the integrated power at each time step using the formula $P(t) = a\int_\Omega \sum_{g=1}^{G} \Sigma_{f,g}\phi_g d\boldsymbol{x}$, where $a$ is the normalization coefficient that correlates to a certain integrated power value.

## 4.1 One group test

Let's look at the little PWR reactor ($\Omega$ – reactor core area) 2D testing challenge. Figure 3 depicts the geometrical model of a small PWR reactor core. The fuel rod's diameter

is 0.82 cm, and the cell width is 1.26 cm. Tab. 1 displays the standard notation for neutronics constants. Fuels for cassettes come in two varieties: 1% $UO_2$ and 2% $UO_2$. $\beta = 6.5 \cdot 10^{-3}$, $\lambda = 0.08$ s$^{-1}$, and $v = 5 \cdot 10^5$ cm/s are the parameters for delayed neutrons that are employed. At the domain's edge, the reflective boundary condition is established.

We have 49 vertices in the coarse grid and 115891 vertices in the fine grid. The computation continues until $T = 0.4$ seconds. For both grids, the time step is $\tau = 0.001$. A fine-grid solution is what we consider to be an exact solution. 1.18398 is $K_{eff}$'s starting value.

Let's determine the process's next scenario:

- Solve the $\lambda$-spectral problem;
- As the initial condition, take the solution of the $\lambda$-spectral problem;
- At time $t = 0.1$ sec, change the removal cross-section $\Sigma_r$ for fuel in zone 1 by +2% (simulation of immersion of control rods);
- At time $t = 0.3$ sec, change the removal cross-section $\Sigma_r$ for fuel in zone 1 by -3% (simulation of withdrawal of control rods).

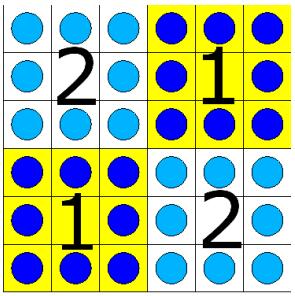


Figure 3: Geometrical model of the small PWR-2D reactor core

Fig. 4 displays the integral power for the fine grid as well as the relative errors (%) of the integral powers. The error is more than 10% when using four or fewer multiscale basis functions, while it is less than 1% when using 16 or more.

Figures show a comparison of the multiscale solution's relative $L_2$ and $H_1$ errors over time for a variety of multiscale basis functions. 5, 6. As long as we use a sufficient number of multiscale basis functions, the numerical results show good convergence.

Tab. 2 displays the relative $L_2$ and $H_1$ errors at the final time for various multiscale basis functions. For instance, we get 0.71% for the $L_2$ error and 4.34% for the $H_1$ error for the pseudo 0th moment of angular flux when we apply 16 multiscale basis functions. Furthermore, the relative errors for the second instant of angular flux for $L_2$ and $H_1$ are 0.81% and 2.56%, respectively. According to calculations, at least 16 multiscale basis functions must be used. Fig. 7 displays the multiscale and fine-grid solutions for varying numbers of bases (on each local domain $\omega_i$) for pseudo 0th moment of angular flux at the final time.

## 4.2 Two group test

The TWIGL two-dimensional transport test is taken into account. A fourth of the reactor core, measuring 160 by 160 cm, is modeled. The geometrical model of the core, which displays different kinds of fuel assemblies, is displayed in Fig. 8. The vacuum boundary condition is established at the reactor core's outer edge. Tab. 3 contains the neutronics constants in the standard notations. The entire medium and $\chi_1 = 1$, $\chi_2 = 0$ have the same fission spectra for prompt and delayed neutrons. One set of delayed neutrons with an effective percentage of $\beta = 0.0075$ and a decay constant of $\lambda = 0.08\,\mathrm{s}^{-1}$ are employed. $v_1 = 10^7$ cm/s and $v_2 = 2 \cdot 10^5$ cm/s are the neutron velocities.

Table 1: Neutronics constants for small PWR-2D.

| Material | 1 | | 2 | |
|---|---|---|---|---|
| | coolant | fuel | coolant | fuel |
| $D$ | 0.34474 | 0.77002 | 0.31679 | 0.80236 |
| $\Sigma_t$ | 0.96691 | 0.43288 | 1.05221 | 0.41543 |
| $\Sigma_r$ | 0.00538 | 0.08933 | 0.00606 | 0.06627 |
| $\Sigma_f$ | 0.0 | 0.05473 | 0.0 | 0.03337 |
| $\nu$ | 0.0 | 2.44844 | 0.0 | 2.45482762 |

Table 2: Relative $L_2$ and $H_1$ errors (%) at final time.

| Bases | DOF | Pseudo 0th moment | | Second moment | | Calc time |
|---|---|---|---|---|---|---|
| | | $L_2$ error | $H_1$ error | $L_2$ error | $H_1$ error | |
| 1 | 49 | 99.97 | 99.99 | 99.97 | 99.99 | 0.03 |
| 2 | 98 | 99.83 | 99.90 | 99.84 | 99.90 | 0.05 |
| 4 | 196 | 25.61 | 34.38 | 26.65 | 27.64 | 0.10 |
| 8 | 392 | 2.64 | 8.99 | 2.80 | 4.65 | 0.35 |
| 16 | 784 | 0.71 | 4.34 | 0.81 | 2.56 | 1.15 |
| 32 | 1568 | 0.07 | 1.28 | 0.14 | 1.17 | 6.66 |
| fine | 115891 | – | – | – | – | 815.00 |

Table 3: Neutronics constants for TWIGL-2D.

| Material | 1 | 2 | 3 |
|---|---|---|---|
| $\Sigma_{t,1}$ | 0.2481 | 0.2481 | 0.2644 |
| $\Sigma_{t,2}$ | 0.9833 | 0.9833 | 0.7167 |
| $\Sigma_{r,1}$ | 0.01 | 0.01 | 0.008 |
| $\Sigma_{r,2}$ | 0.15 | 0.15 | 0.05 |
| $\Sigma_{s,1\to2}$ | 0.01 | 0.01 | 0.01 |
| $\Sigma_{s,1\to1}$ | 0.2281 | 0.2281 | 0.2464 |
| $\Sigma_{s,2\to2}$ | 0.8333 | 0.8333 | 0.6667 |
| $\nu_1\Sigma_{f,1}$ | 0.007 | 0.007 | 0.003 |
| $\nu_2\Sigma_{f,2}$ | 0.2 | 0.2 | 0.06 |

Table 4: Relative $L_2$ errors (%) at final time.

| Bases | DOF | $L_2$ error | | | | Calc time |
|---|---|---|---|---|---|---|
| | | $\phi_{ms_{0,1}}$ | $\phi_{ms_{2,1}}$ | $\phi_{ms_{0,2}}$ | $\phi_{ms_{2,2}}$ | |
| 1 | 121 | 54.64 | 54.88 | 54.70 | 64.23 | 1.70 |
| 2 | 242 | 21.55 | 21.69 | 21.55 | 26.80 | 4.15 |
| 4 | 484 | 12.93 | 12.88 | 12.96 | 16.39 | 12.61 |
| 8 | 968 | 2.97 | 3.14 | 2.96 | 4.44 | 45.12 |
| 16 | 1936 | 0.09 | 0.11 | 0.09 | 0.06 | 165.36 |
| 32 | 3872 | 0.01 | 0.01 | 0.01 | 0.05 | 690.30 |
| fine | 25921 | – | – | – | – | 6590.00 |

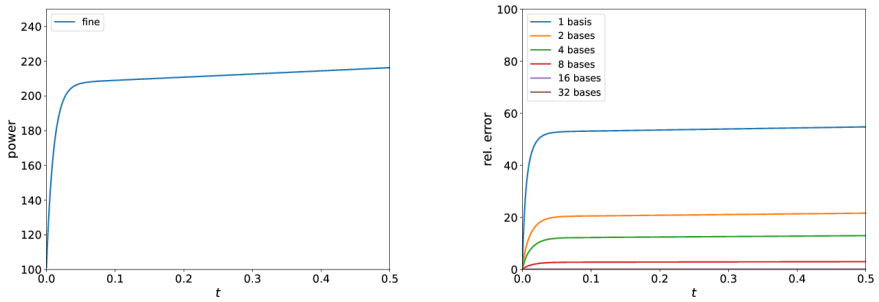


Figure 4: Integral power of fine frid solution and relative errors (%) of the integral power of multiscale solution with different number of basis functions.

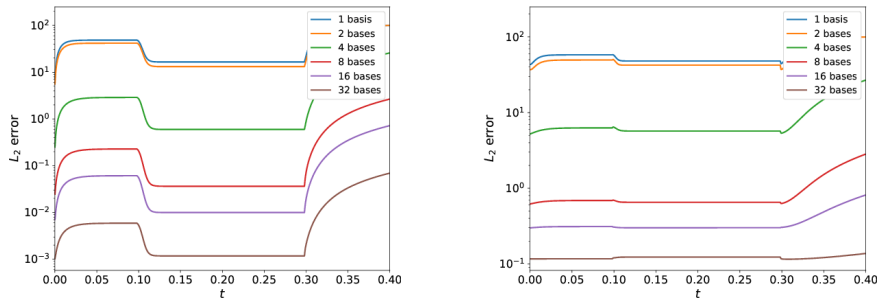


Figure 5: Relative $L_2$ errors (%) of the multiscale angular flux

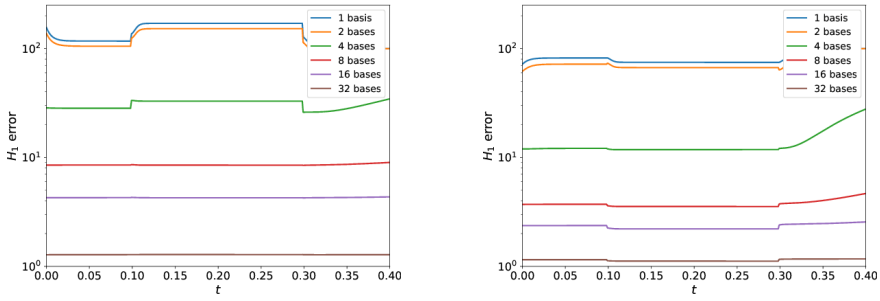


Figure 6: Relative $H_1$ errors (%) of the multiscale angular flux

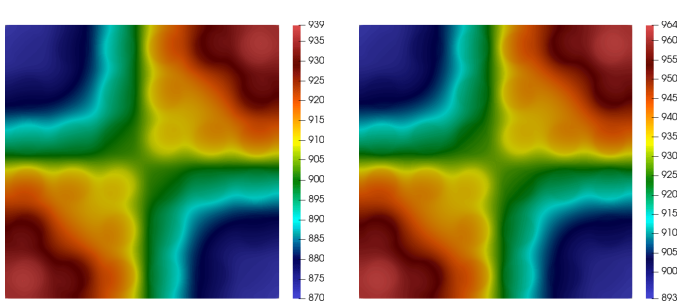

Figure 7: Fine-grid and multiscale solutions at final time for pseudo 0th moment of angular flux

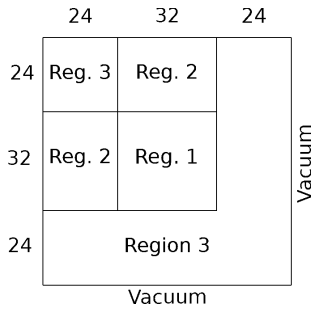


Figure 8: Geometrical model of 1/4 reactor core TWIGL-2D.

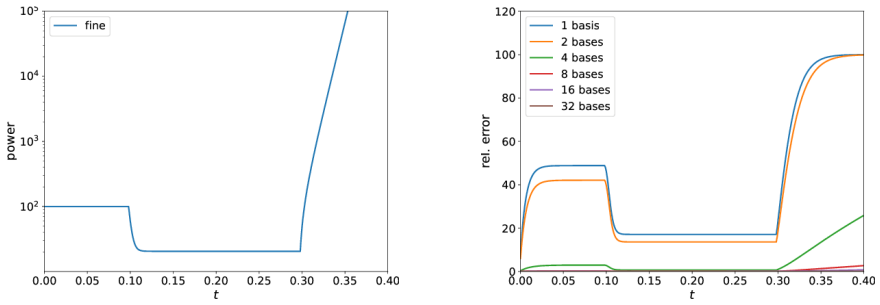


Figure 9: Integral power (fine grid) and relative errors (%) of the multiscale solution power.

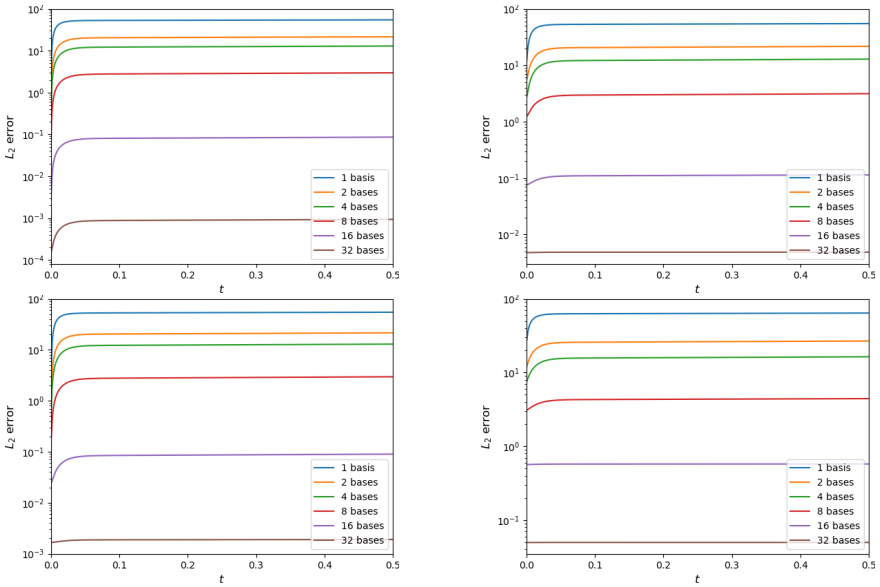


Figure 10: Relative $L_2$ errors (%) of the multiscale solution

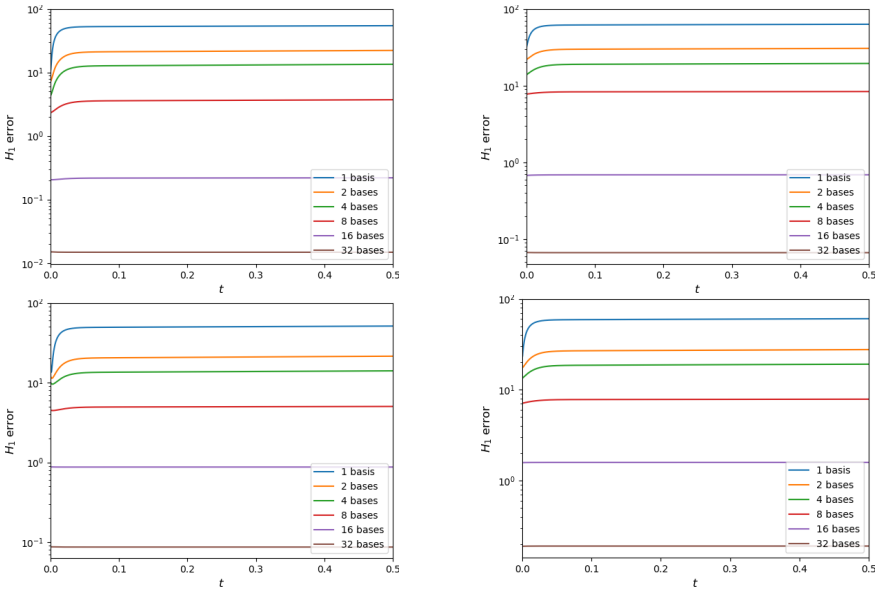


Figure 11: Relative $H_1$ errors (%) of the multiscale solution

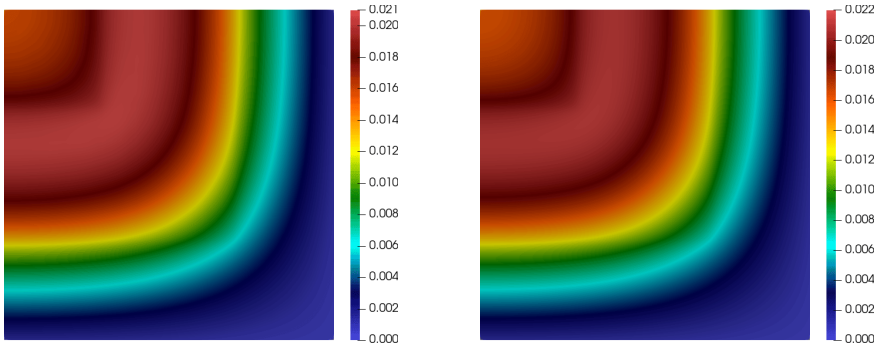


Figure 12: Fine-grid and multiscale solutions at final time for pseudo 0th moment of angular flux

We have 121 vertices in the coarse grid and 25921 vertices in the fine grid. The computation continues until $T = 0.5$ seconds. For both grids, the time step is $\tau = 0.0001$. We use the fine-grid solution as an exact solution. $K_{eff}$ has an initial value of 0.916075.

The test case of dynamic process:

- Solve the $\lambda$-spectral problem;
- As the initial condition, take the solution of the $\lambda$-spectral problem;
- At time $t = 0$ sec, change the removal cross-section $\Sigma_{r,2}$ for region 1 by 0.0035 $\text{cm}^{-1}$ (simulation of withdrawal of control rods).

Figure 9 shows the integral power for the fine grid and the relative errors (%) of integral powers. Using four or more multiscale basis functions results in an inaccuracy of less than 3Figures 10 and 11 depict the relative $L_2$ and $H_1$ errors of the multiscale solution with time for varied numbers of multiscale basis functions. For multiscale solutions, we now employ the following notation: $\phi_{ms_{0,1}}$– pseudo 0th moment of fast (group 1) energy group's angular flux; $\phi_{ms_{2,1}}$ – fast energy group's second instant of angular flux; $\phi_{ms_{0,2}}$– pseudo 0th moment of thermal (group 2) energy group's angular flux; $\phi_{ms_{2,2}}$ – the thermal energy group's second instant of angular flux. The numerical findings show good convergence behavior if a large number of multiscale basis functions are taken.

The relative $L_2$ errors at final time for a variety of multiscale basis functions are shown in Table. 4. For instance, we get 0.71% for the $L_2$ error and 4.34% for the $H_1$ error for the pseudo 0th moment of angular flux when we apply 16 multiscale basis functions. Furthermore, the relative errors for the second instant of angular flux for $L_2$ and $H_1$ are 0.81% and 2.56%, respectively. According to calculations, at least 16 multiscale basis functions must be used. Fig. 12 displays the multiscale and fine-grid solutions for varying numbers of bases (on each local domain $\omega_i$) for pseudo 0th moment of angular flux at the final time.

## 5 Conclusions

In this research we developed a model reduction procedure for neutron transport model based on Generalized Multiscale Finite Element method. We presented a GMsFEM

technique that uses coupled multiscale basis functions for each neutron group. The results showed that GMsFEM performed well in all circumstances. In this study, we looked at a popular and simple form of the neutron transport equation. Even with modern computers, computational costs remain a concern.

# Acknowledgements

D.S. Spiridonov's work is supported by the grant of Russian Science Foundation No. 23-71-30013(https://rscf.ru/project/23-71-30013/) and within the framework of Grant No. FSRG-2024-0003 of the Ministry of Science and Higher Education of the Russian Federation.

# References

[1] James J Duderstadt and Louis J Hamilton. *Nuclear reactor analysis*. Wiley, 1976.

[2] Weston M Stacey. *Nuclear reactor physics*. John Wiley & Sons, 2018.

[3] G Verdú, D Ginestar, V Vidal, and JL Muñoz-Cobo. 3d $\lambda$-modes of the neutron-diffusion equation. *Annals of Nuclear Energy*, 21(7):405–421, 1994.

[4] Alexander V Avvakumov, Valery F Strizhov, Petr N Vabishchevich, and Alexander O Vasilev. Spectral properties of dynamic processes in a nuclear reactor. *Annals of Nuclear Energy*, 99:68–79, 2017.

[5] JL Munoz-Cobo, R Miró, Aaron Wysocki, and A Soler. 3d calculation of the lambda eigenvalues and eigenmodes of the two-group neutron diffusion equation by coarse-mesh nodal methods. *Progress in Nuclear Energy*, 110:393–409, 2019.

[6] Sandra Dulla, Ernest H Mund, and Piero Ravetto. The quasi-static method revisited. *Progress in Nuclear Energy*, 50(8):908–920, 2008.

[7] A Carreño, Antoni Vidal-Ferràndiz, D Ginestar, and G Verdú. Modal methods for the neutron diffusion equation using different spatial modes. *Progress in Nuclear Energy*, 115:181–193, 2019.

[8] Alexander V Avvakumov, Valery F Strizhov, Petr N Vabishchevich, and Alexander O Vasilev. State change modal method for numerical simulation of dynamic processes in a nuclear reactor. *Progress in Nuclear Energy*, 106:240–261, 2018.

[9] M Vasilyeva and DA Stalnov. Numerical averaging for the heat conduction problem in inhomogeneous and perforated media. *Herald of MK Ammosov Northeastern Federal University*, 2017.

[10] Nikolai Sergeevich Bakhvalov and Grigory Panasenko. *Homogenisation: averaging processes in periodic media: mathematical problems in the mechanics of composite materials*, volume 36. Springer Science & Business Media, 2012.

[11] Antoni Vidal-Ferràndiz, S González-Pintor, Damián Ginestar, Christophe Demazière, and Gumersindo Verdú. Pin-wise homogenization for spn neutron transport approximation using the finite element method. *Journal of Computational and Applied Mathematics*, 330:806–821, 2018.

[12] Alexey Talonov and Maria Vasilyeva. On numerical homogenization of shale gas transport. *Journal of Computational and Applied Mathematics*, 301:44–52, 2016.

[13] Yalchin Efendiev and Thomas Y Hou. *Multiscale finite element methods: theory and applications*, volume 4. Springer Science & Business Media, 2009.

[14] Yalchin Efendiev and Thomas Y Hou. Multiscale finite element methods: theory and applications. 4, 2009.

[15] Grégoire Allaire and Robert Brizzi. A multiscale finite element method for numerical homogenization. *Multiscale Modeling & Simulation*, 4(3):790–812, 2005.

[16] Arif Masud and RA2203991 Khurram. A multiscale finite element method for the incompressible navier–stokes equations. *Computer Methods in Applied Mechanics and Engineering*, 195(13-16):1750–1777, 2006.

[17] Thomas Y Hou and Xiao-Hui Wu. A multiscale finite element method for elliptic problems in composite materials and porous media. *Journal of computational physics*, 134(1):169–189, 1997.

[18] Ibrahim Y Akkutlu, Yalchin Efendiev, and Maria Vasilyeva. Multiscale model reduction for shale gas transport in fractured media. *Computational Geosciences*, 20:953–973, 2016.

[19] Uygulaana Kalachikova, Maria Vasilyeva, Isaac Harris, and Eric T Chung. Generalized multiscale finite element method for scattering problem in heterogeneous media. *Journal of Computational and Applied Mathematics*, 424:114977, 2023.

[20] Yalchin Efendiev, Juan Galvis, and Thomas Y Hou. Generalized multiscale finite element methods (gmsfem). *Journal of Computational Physics*, 251:116–135, 2013.

[21] Aleksei Tyrylgin, Maria Vasilyeva, Denis Spiridonov, and Eric T Chung. Generalized multiscale finite element method for the poroelasticity problem in multicontinuum media. *Journal of Computational and Applied Mathematics*, 374:112783, 2020.

[22] Denis Spiridonov, Maria Vasilyeva, and Eric T Chung. Generalized multiscale finite element method for multicontinua unsaturated flow problems in fractured porous media. *Journal of Computational and Applied Mathematics*, 370:112594, 2020.

[23] Patrick Jenny, Seong H Lee, and Hamdi A Tchelepi. Adaptive multiscale finite-volume method for multiphase flow and transport in porous media. *Multiscale Modeling & Simulation*, 3(1):50–64, 2005.

[24] Irina Sokolova, Muhammad Gusti Bastisya, and Hadi Hajibeygi. Multiscale finite volume method for finite-volume-based simulation of poroelasticity. *Journal of Computational Physics*, 379:309–324, 2019.

[25] Maria Vasilyeva and Denis Spiridonov. Multiscale model reduction with local online correction for polymer flooding process in heterogeneous porous media. *Mathematics*, 11(14):3104, 2023.

[26] Eric T Chung, Wing Tat Leung, and Maria Vasilyeva. Mixed gmsfem for second order elliptic problem in perforated domains. *Journal of Computational and Applied Mathematics*, 304:84–99, 2016.

[27] Valentin Alekseev, Qili Tang, Maria Vasilyeva, Eric T Chung, and Yalchin Efendiev. Mixed generalized multiscale finite element method for a simplified magnetohydrodynamics problem in perforated domains. *Computation*, 8(2):58, 2020.

[28] Eric T Chung, Yalchin Efendiev, Wing Tat Leung, Maria Vasilyeva, and Yating Wang. Non-local multi-continua upscaling for flows in heterogeneous fractured media. *Journal of Computational Physics*, 372:22–34, 2018.

[29] Maria Vasilyeva, Eric T Chung, Yalchin Efendiev, and Jihoon Kim. Constrained energy minimization based upscaling for coupled flow and mechanics. *Journal of Computational Physics*, 376:660–674, 2019.

[30] Maria Vasilyeva, Eric T Chung, Siu Wun Cheung, Yating Wang, and Georgy Prokopev. Nonlocal multicontinua upscaling for multicontinua flow problems in fractured porous media. *Journal of Computational and Applied Mathematics*, 2019.

[31] Eric T Chung, Yalchin Efendiev, and Wing Tat Leung. Constraint energy minimizing generalized multiscale finite element method. *Computer Methods in Applied Mechanics and Engineering*, 339:298–319, 2018.

[32] DA Spiridonov and J Huang. An online generalized multiscale finite element method for dual-continuum unsaturated filtration problem in domains with rough boundaries. *Lobachevskii Journal of Mathematics*, 44(10):4170–4182, 2023.

[33] Dmitry Ammosov, Yalchin Efendiev, Elena Grekova, and Maria Vasilyeva. Generalized macroscale model for cosserat elasticity using generalized multiscale finite element method. *Journal of Computational Physics*, 461:111011, 2022.

[34] Yalchin Efendiev, Juan Galvis, and Thomas Y Hou. Generalized multiscale finite element methods (gmsfem). *Journal of computational physics*, 251:116–135, 2013.

[35] Denis Spiridonov, Maria Vasilyeva, and Wing Tat Leung. A generalized multiscale finite element method (gmsfem) for perforated domain flows with robin boundary conditions. *Journal of Computational and Applied Mathematics*, 357:319–328, 2019.

Spiridonov D.A.,
North-Eastern Federal University,
Russia, 677000 Yakutsk, Kulakovskogo street, 42,
Email: d.stalnov@mail.ru.

Received 22.06.2024 , Accepted 30.07.2024, Available online 31.03.2025.